Further insight on recombination losses in the intrinsic layer of a-Si:H solar cells using computer modeling tools

Francisco A. Rubinelli, Helena Ramirez, Carlos M. Ruiz, and Javier A. Schmidt

Citation: Journal of Applied Physics **121**, 184502 (2017); doi: 10.1063/1.4983010
View online: http://dx.doi.org/10.1063/1.4983010
View Table of Contents: http://aip.scitation.org/toc/jap/121/18
Published by the American Institute of Physics

Further insight on recombination losses in the intrinsic layer of a-Si:H solar cells using computer modeling tools

Francisco A. Rubinelli,[1,a)] Helena Ramirez,[2] Carlos M. Ruiz,[1] and Javier A. Schmidt[2,b)]
[1]*Instituto de Desarrollo Tecnológico para la Industria Química (INTEC), Universidad Nacional del Litoral (UNL), CONICET, Güemes 3450, 3000 Santa Fe, Argentina*
[2]*Instituto de Física del Litoral (IFIS-Litoral), Universidad Nacional del Litoral (UNL), CONICET, Güemes 3450, 3000 Santa Fe, Argentina*

(Received 11 October 2016; accepted 22 April 2017; published online 9 May 2017)

Recombination losses of a-Si:H based *p-i-n* solar cells in the annealed state are analyzed with device computer modeling. Under AM1.5 illumination, the recombination rate in the intrinsic layer is shown to be controlled by a combination of losses through defect and tail states. The influence of the defect concentration on the characteristic parameters of a solar cell is analyzed. The impact on the light current-voltage characteristic curve of adopting very low free carrier mobilities and a high density of states at the band edge is explored under red and AM1.5 illumination. The distribution of trapped charge, electric field, and recombination loses inside the intrinsic layer is examined, and their influence on the solar cell performance is discussed. Solar cells with intrinsic layers deposited with and without hydrogen dilution are examined. It is found that the photocurrent at −2 V is not always a good approximation of the saturated reverse-bias photocurrent in a-Si:H *p-i-n* solar cells at room temperature. The importance of using realistic electrical parameters in solar cell simulations is emphasized. *Published by AIP Publishing*. [http://dx.doi.org/10.1063/1.4983010]

I. INTRODUCTION

Amorphous silicon cell technology has considerably evolved during the last few decades. Scientists worldwide have developed high quality alloys based on hydrogenated amorphous silicon and microcrystalline silicon. The technological potential of each form is remarkable as their electronic properties can be preserved and tailored by incorporating hydrogen into the network with an appropriate concentration and bonding structure. Amorphous and microcrystalline silicon thin films are currently applied in solar cells and numerous other electronic devices like transistors, optical detectors, color sensors, and image and printing arrays, among others.

The simulation of the electrical and optical behavior of semiconductor devices has been established as an essential tool for the improvement of existing devices and the development of new ones. Device modeling involves the numerical solution of differential equations that mathematically describes the device operation. The input parameters are obtained from material and device research. The accurate calibration of these parameters, based on the comparison between simulated and experimental device characteristic curves, is an essential step in computer modeling. The calibrated code can be used as a predictive tool after reproducing a broad range of experimental results. Solar cell structures can be tested and optimized for their best performance. When no agreement between simulated and measured data can be reached, the modeling used to describe the material properties and device transport needs to be refined. The multiple tasks associated with computer modeling contribute to a better understanding of the optical and electrical transport physics and allow checking the sensitivity of the device performance to parameters that cannot be easily measured.

The traditional method followed in solar cell modeling is a three step procedure. The initial step is to run simulations with electrical and optical parameters measured with thin film techniques like dark conductivity, photoconductivity, transmittance and reflectance, Constant Photocurrent Method (CPM), Space Charge Limited Current (SCLC), Electron Spin Resonance, and/or taken from literature. Thin film experimental techniques provide the activation energy, optical band gap, absorption coefficient, global defect density, and valence band tail slope, in each device layer. The second step is the fitting of Current-Voltage curves (*J-V*) and/or Spectral Responses (SR) of well-behaved solar cells in order to calibrate parameters that are more difficult to measure, like capture cross sections, effective density of states, conduction band tail slope, and so on. The third step is to achieve fine calibration by simultaneously matching experimental data of several solar cell structures deposited under similar conditions but with different intrinsic layer thicknesses and/or measured at different temperatures. The more curves are successfully fitted the more reliable the input parameters become.

II. MOTIVATIONS

Some researchers have the erroneous idea that the high number of input parameters used in solar cell computer modeling allows for the fitting of any characteristic curve. That is not the case, since several parameters are provided by experiments and the rest can be varied only within a reasonable range given by the literature. Analytical or approximated methods used by experimentalists usually rely on a considerably lower number of parameters. However, the use of a reduced number of parameters does not mean that the

a)Deceased
b)E-mail: javier.schmidt@santafe-conicet.gov.ar

others do not exist; it means that arbitrary values are implicitly assigned to those parameters, assuming that hopefully they will not impact the final results. In addition, the choice of ignoring these parameters could hide valuable information that could be used for the optimization of solar cell structures.

The common practice is to employ the highest possible number of measured parameters as inputs. However, sometimes parameters resolved with thin film measurement techniques cannot be effectively incorporated into solar cell modeling, because the fittings of experimental *J-V* or *SR* curves cannot be achieved. This is an indirect proof that even playing with the numerous input parameters used in computer modeling it is not always possible to match the solar cell characteristic curves. In these particular situations, the assumptions made in the simplified models used by experimentalists could be revised, and an interesting feedback between experiments and computer simulations could take place. For instance, the mobility gap of 1.89–1.9 eV reported in 1989 for intrinsic hydrogenated amorphous silicon (a-Si:H)[1] made the reproduction of the Fill Factor (*FF*) of *p*-SiC:H/buffer/*i*-a-Si:H/*n*-a-Si:H structures very difficult. The open circuit voltage (V_{OC}) and short circuit current (J_{SC}) could be matched, but the predicted *FF* was always lower than the *FF* experimentally reported.[2] Several scenarios were explored, like low electron front contact barriers, different gaps and low doping concentrations in the (*p*)a-SiC:H layer, higher defect state densities in the (*i*)a-Si:H layer, different *p*/*i* and *i*/*n* interface layers, etc., in order to decrease V_{OC} when the mobility gap was increased from 1.72 to 1.9 eV. These ideas led to the reproduction of V_{OC} at the expense of severe losses in the *FF*. The matching of the experimental V_{OC} and *FF* could only be achieved by assuming the presence of a highly defective thin layer at the *p*/*i* interface with a mobility gap of 1.72 eV, so that V_{OC} and *FF* became controlled by recombination losses taking place at this defective layer rather than at the intrinsic bulk layer.[2] Nevertheless, the presence of such a defective layer at the *p*/*i* interface could not be justified by physical grounds. The experimental mobility gap E_G was determined using internal photoemission at metal/(i)-a-Si:H Schottky barriers.[1] More recently, Kind *et al.*,[3] by studying the thermal ideality factor of dark *J-V* characteristics of a-Si:H *p-i-n* structures with different intrinsic layer thicknesses obtained a lower mobility gap of 1.69 eV, being 1.72 eV the most accepted value in the literature that allows for a natural matching of the a-Si:H solar cell light *J-V* curves. Other examples of curious experimental electrical parameters can be found in the contribution of Liang *et al.*,[4] where temperature-dependent measurements combined with computer modeling of a thickness series of hydrogenated a-Si:H *n-i-p* solar cells in the annealed and light soaked states were presented.[4] Assuming unusually high values for the density of states at band edges, and very low free carrier mobilities – extracted from drift mobilities obtained with the Time of Flight (TOF) technique, they concluded that the density of defect states in the intrinsic layer is sufficiently low in annealed solar cells to neglect its effect on the solar cell efficiency, η.[4] The strong temperature dependence of the hole drift mobility in a-Si:H provides, according to the authors, the needed evidence to explain the cell efficiency as a function of temperature and establish that hole drift mobilities determine the largest values of the maximum power that can be obtained from a-Si:H based solar cells.[5] Their work captured our attention for several reasons: (a) their simulations were performed with the computer code AMPS-1D of Pennsylvania State University.[6,7] Our software D-AMPS-1D (Refs. 8–12) is based on the AMPS-1D source code, (b) some of their electrical parameters are unusual, (c) fittings of experimental *J-V* curves under illuminated conditions are not fully shown: only V_{OC} and the ratio between the maximum power density P_{MAX} and the photocurrent J_P measured at a reverse voltage of −2 V were really matched, (d) no fittings of dark *J-V* curves were included, (e) red laser instead of the AM1.5 light source was used, and (f) the maximum power density of the as-deposited a-Si:H cells is believed to have achieved the hole-mobility limit established by valence band-tail trapping; i.e., defect states did not limit their efficiency.

In this contribution, the results obtained by Liang *et al.*[4] for a-Si:H solar cells in the annealed state are discussed. This paper is organized as follows: in Sec. III the solar cell structures, electrical parameters, and computer codes used by both groups are compared. In Secs. IV–VI, the contribution of tail and defect states to the total recombination rate and to the shape of the *J-V* curve under red and AM1.5 illumination is explored in a-Si:H *p-i-n* structures. Dark *J-V* curves are also analyzed. Our conclusions indicate that defect states do have a significant impact on the *FF* and V_{OC} of the as-deposited a-Si:H based solar cells, in disagreement with Liang *et al.*'s findings.

III. COMPARISON OF ELECTRICAL PARAMETERS AND SOLAR CELL DEVICES

Our simulations were performed with the computer code D-AMPS (Analysis of Microelectronic and Photonic Devices + New Developments) that solves the system of three nonlinear equations (Poisson's equation and continuity equations for free electrons and holes) with the finite difference method and the Newton-Raphson technique.[6,7] The independent variables are the electron potential and the quasi-Fermi levels. D-AMPS is an updated version of the well-known software AMPS that includes extra features like amphoteric states, Defect Pool-model (DPM), and Pool-Frenkel effect, a simplified treatment of light scattering, among others.[8–12]

A. Solar cell devices: Experimental and simulated performances

In previous contributions,[13,14] the *J-V* curves of a-Si:H based devices were analyzed with D-AMPS under dark and illuminated conditions. Our parameters were calibrated by fitting experimental *J-V* characteristic curves of *p-i-n* junctions with intrinsic layer thicknesses of 200, 400, and 600 nm. Samples were deposited in a multi-chamber RF-PECVD facility from MV Systems at Delft University that contains four processing chambers and a load lock to avoid contamination at interfaces. The full device structure is: *(80 nm)TCO/(10 nm)p-a-SiC:H/(200-400-600 nm)i-a-Si:H/*

(20 nm)n-a-Si:H/(300 nm)Al, where TCO stands for Transparent Conductive Oxide. Films were deposited at a substrate temperature of 180 °C, a pressure of 0.6 mbar (*n*-layer) or 0.7 mbar (*p*-, *i*-layer), and a RF power of 25 mW/cm^2 on a textured Asahi U-type substrate and front contact.[3] The deposition rates were 0.2 nm/s for the *p*- and *i*-layers, and 0.1 nm/s for the *n*-layer. The Al back contact was deposited by evaporation in a PROVAC single chamber system. Samples were finally annealed for 30 min at 130 °C. Devices with an extra 5-nm-thick silicon carbide buffer layer at the *p*/*i* interface were also analyzed with a similar methodology,[14] but in this contribution solar cells with no buffer layer will be discussed as in Liang *et al.*'s paper.[4] Experimental dark and light *J-V* curves of the a-Si:H *p-i-n* devices and their corresponding fittings can be found elsewhere.[13] The electrical parameters obtained from our fittings are listed in the second column of Table I. In our simulations, doping densities and Gaussian peak positions were adjusted to reproduce the experimental activation energies of each device layer. Optical parameters were obtained from measured reflection and transmission spectra of a-Si:H films. The global density of states and the Urbach valence band tail slope were extracted with the technique of Dual Beam Photoconductivity (DBP). The optical modeling of D-AMPS takes into account scattering at rough surfaces and the absorption of light at external contacts; multiple reflections at interfaces are evaluated with the Fresnel's equations; refractive indexes change with wavelength; all aspects that were not included in the original version of AMPS-1D used by Liang *et al.*[4]

Figure 1 shows the experimental (solid symbols) and simulated (open symbols) performances of *p-i-n* solar cells fabricated at Delft University for 200, 400, and 600 nm thick intrinsic layers. The thickest sample corresponds to the performance predicted by D-AMPS for a hypothetical sample with the 893-nm-thick intrinsic layer, using the electrical parameters obtained for the sample with the 600-nm-thick intrinsic layer. It can be seen that J_{SC} increases steadily, while V_{OC} remains essentially constant as the thickness increases in this range. On the other hand, *FF* decreases monotonically and the efficiency reaches a maximum value for an i-layer thickness around 600 nm. The experimental trends are very well reproduced by the simulations, being the simulated points always within the error bars of the experimental points. This agreement, in addition to the accurate description of the dark *J-V* characteristic curves, is an indication that the parameters describing the solar cell behavior are well calibrated.

Liang *et al.*'s *a*-Si:H *n-i-p* solar cells were also grown with the RF glow discharge technique but on stainless steel substrates. Their *n* and *p* layers were the same in all of depositions; the deposition time for the intrinsic layer was chosen to give intrinsic layer thicknesses of 183, 377, 574, and

TABLE I. The meaning of the symbols of the first column is as follows: W intrinsic layer thickness, E_G mobility gap, N_c and N_v effective density of states at the conduction and valence band, G_{AO} and G_{DO} density of states at the conduction and valence band edges, μ_N and μ_P electron and hole mobilities, E_D and E_A valence and conduction band-tail slopes, $\sigma_{NA\text{-}T}$, $\sigma_{PA\text{-}T}$, and $\sigma_{ND\text{-}T}$, $\sigma_{PD\text{-}T}$ capture cross sections at acceptor-like (A) and donor like (D) tail states for electrons (N) and holes (P), D^-, D^0, and D^+ densities of states enclosed in the three Gaussians (UDM), E^-, E^0, and E^+ Gaussian peak positions associated with the (+/0) transitions, s_D standard deviations, $\sigma_{NA\text{-}G}$, $\sigma_{PA\text{-}G}$ and $\sigma_{ND\text{-}G}$, $\sigma_{PD\text{-}G}$ capture cross sections at acceptor-like (A) and donor like (D) defect states for electrons (N) and holes (P). Second column: electrical parameters obtained by fitting dark and light *J-V* curves of undiluted a-Si:H *p-i-n* solar cells grown at Delft University. Third column: electrical parameters proposed by Liang *et al.*[4] Fourth column: parameters obtained by matching the light *J-V* reported by Liang *et al.* for the diluted a-Si:H *n-i-p* sample with an 893 nm thick intrinsic layer.

Intrinsic layer parameters	Undiluted a-Si:H delft values	Diluted a-Si:H Liang *et al.*	Diluted a-Si:H our values
W (nm)	200–400–600	893 and others	893
E_G (eV)	1.72	1.74	1.88
N_C, N_V (cm^{-3})	3×10^{20}	4×10^{20}	4×10^{19}
G_{AO} (cm^{-3} eV^{-1})	1×10^{21}	1.6×10^{22}	7×10^{20}
G_{DO} (cm^{-3} eV^{-1})	1×10^{21}	6×10^{21}	7×10^{20}
μ_N (cm^2 V^{-1} s^{-1})	20	2	10
μ_P (cm^2 V^{-1} s^{-1})	3.5	0.2–0.3	1
E_D (meV)	48	40	45
E_A (meV)	30	20	25
$\sigma_{ND\text{-}T}$ (cm^2)	2×10^{-15}	1×10^{-16}	2×10^{-15}
$\sigma_{PD\text{-}T}$ (cm^2)	1×10^{-16}	1.3×10^{-16}	2×10^{-17}
$\sigma_{NA\text{-}T}$ (cm^2)	1×10^{-16}	1.3×10^{-16}	2×10^{-17}
$\sigma_{PA\text{-}T}$ (cm^2)	2×10^{-15}	Not specified	2×10^{-15}
D^- (cm^{-3}) (+/0 and 0/−)	$4.8\text{–}4.4\text{–}3.6 \times 10^{15}$	Not specified	8.8×10^{14}
D^0 (cm^{-3}) (+/0 and 0/−)	$2.4\text{–}2.2\text{–}1.8 \times 10^{15}$	Not specified	4.4×10^{14}
D^+ (cm^{-3}) (+/0 and 0/−)	$4.8\text{–}4.4\text{–}3.6 \times 10^{15}$	Not specified	8.8×10^{14}
$E_D{}^-$ (eV) (+/0, $U = 0.2$ eV)	0.55	Not specified	0.62
$E_D{}^0$ (eV) (+/0, $U = 0.2$ eV)	0.85	Not specified	0.92
$E_D{}^+$ (eV) (+/0, $U = 0.2$ eV)	1.15	Not specified	1.22
s_D (eV)	0.13	Not specified	0.13
$\sigma_{ND\text{-}G}$ (cm^2)	9×10^{-15}	4×10^{-15}	9×10^{-15}
$\sigma_{PD\text{-}G}$ (cm^2)	$8\text{–}7.3\text{–}3.5 \times 10^{-16}$	7.5×10^{-16}	9×10^{-16}
$\sigma_{NA\text{-}G}$ (cm^2)	$8\text{–}7.3\text{–}3.5 \times 10^{-16}$	Not specified	9×10^{-16}
$\sigma_{PA\text{-}G}$ (cm^2)	9×10^{-15}	Not specified	9×10^{-15}

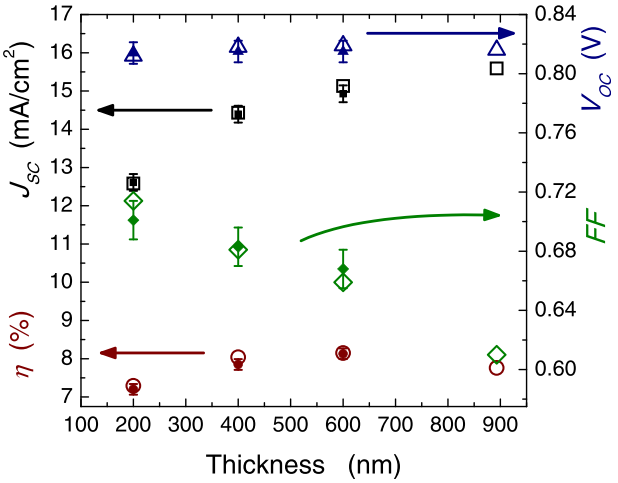

FIG. 1. Comparison of experimental (solid symbols) and simulated (open symbols) solar cells performances of a-Si:H *p-i-n* samples deposited at Delft University, characterized by J_{SC} (squares, left scale), V_{OC} (triangles, right scale), FF (diamonds, right scale), and efficiency (circles, left scale). The rightmost points correspond to the performance obtained for a *p-i-n* solar cell with an 893-nm-thick intrinsic layer using the electrical parameters obtained for the 600-nm-thick intrinsic layer (second column of Table I).

893 nm. Liang *et al.*[4] only reported the experimental performance of the solar cell with the 893-nm-thick intrinsic layer. Both our samples and the solar cells deposited by Liang *et al.* were not optimized to achieve the best efficiency; i.e., they do not have a highly reflecting back contact; but interfaces, contacts, and doped layers do no limit the device performance. In Table II, the performance of the 893-nm-thick solar cell studied by Liang *et al.*[4] is presented, together with the results of some simulations performed with different sets of parameters.

The lower J_{SC} of Liang *et al.*'s 893-nm-thick sample (14.40 mA/cm^2, compared to 15.59 mA/cm^2 of the last line of Table II) could be probably due to the use of ITO at the front contact, instead of Asahi U-type (SnO_2:F) TCO as in the samples of Delft University. Higher recombination losses taking place at the intrinsic layer could also contribute to a lower J_{SC}, what would also explain their lower FF (0.559 compared to 0.610). The higher experimental V_{OC} of Liang *et al.*'s sample (0.982 V compared to 0.816 V) is expected due to the high hydrogen dilution used in the preparation of the (*i*)-a-Si:H layer.[4] Details of the deposition procedures were given in a previous publication where a triple-junction silicon alloy cell with 14.6% initial and 13% stabilized efficiency was reported.[15] Curiously, in their Table I of Ref. 4 the a-Si:H mobility gap of the intrinsic layer was assumed 1.74 eV, which is only 0.02 eV higher than 1.72 eV, the gap regularly assumed for intrinsic a-Si:H deposited without hydrogen dilution. The full list of parameters used by Liang *et al.* can be found in the third column of Table I.[4,5,16] In order to reach a V_{OC} of 0.982 V with a mobility gap of $E_G = 1.74$ eV ($V_{OC} \sim 0.816$ V with $E_G = 1.72$ eV, see the last line of Table II) with Liang *et al.*'s parameters, doped layers have to be assumed of extremely good-quality. In this way, the electric field in the intrinsic a-Si:H layer could be strong enough to significantly reduce the recombination losses. By adopting extremely optimistic values of 0.3 and 0.2 eV for the activation energies of the *p*-a-SiC:H and *n*-a-Si:H layers, respectively, assuming neutral boundary conditions, a temperature of only 293 K (20 °C) in order to further increase V_{OC}, and optimizing the optical parameters at rough interfaces, our best result was $V_{OC} \sim 0.953$ V (second line of Table II). The hole mobility was adopted to be 0.25 cm^2 V^{-1} s^{-1}, the average value between the mobilities used by Liang *et al.* in Refs. 4 and 5. The density of dangling bonds (not reported by Liang *et al.* in their simulations[4]) that makes the best compromise between J_{SC}, V_{OC}, and FF was $\sim 5 \times 10^{15}$ cm^{-3}. When higher densities of dangling bonds (DBs) are assumed, the FF can be better matched but J_{SC} drops significantly. The opposite trend is obtained when lower densities of DBs are assumed. The very low hole mobility adopted by Liang *et al.* makes FF and J_{SC} quite sensitive to the density of DBs, in contradiction with their statement that the density of defect levels present in the as-deposited or annealed samples is sufficiently low to have a minor effect on the solar cell efficiency of a-Si:H solar cells. The third line of Table II corresponds to the simulation of the light *J-V* curve of the 893-nm-thick device of Liang *et al.*[4] with different parameters, where the increase of the mobility gap of a-Si:H with hydrogen dilution is taken into account. The list of parameters used to match the experimental light *J-V* curve can be found in the last column of Table I. The parameters of doped layers were assumed identical to the ones used in samples of Delft University. Main differences between our and Liang *et al.*'s parameters are the higher intrinsic a-Si:H mobility gap of 1.88 eV, the Urbach tail slope of 45 meV, the free carrier mobilities of 10 and 1 cm^2 V^{-1} s^{-1} for electrons and holes, and the lower density of states of 7×10^{20} cm^{-3} eV^{-1} at the mobility edges. These simulations will be discussed in detail in Section IV.

In D-AMPS, the density of defects can be modeled with either the Uniform Density Model (UDM), which assumes a constant density of defects inside each device layer,[8] or with the Defect Pool Model (DPM).[9] Defect states can be assumed amphoteric or approximated by pairs of decoupled donor-like and acceptor-like states.[8] In order to facilitate the comparison of the *J-V* curves predicted with our or Liang *et al.*'s parameters, the density of defects was modeled with the UDM and with the decoupled approximation.[8] The UDM is regularly implemented in a-Si:H by means of three pairs of Gaussians, recognized as D^-, D^0, and D^+: three Gaussians with donor-like and three with acceptor-like states, separated in energy by the correlation energy U that

TABLE II. Experimental performance of Liang *et al.*'s *n-i-p* solar cell with an 893 nm thick intrinsic layer (first line), and simulations obtained with Liang *et al.* parameters and optimistic activation energies in doped layers (third column of Table I); with our parameters for hydrogen-diluted (i)-a-Si:H and realistic doped layer activation energies (fourth column of Table I); and with the parameters that simulate the solar cells deposited at Delft University (second column of Table I).

	J_{SC} (mA/cm^2)	V_{OC} (V)	FF	η (%)
Experimental values	14.40	0.982	0.559	7.90
Diluted a-Si:H—Liang *et al.*	14.15	0.953	0.567	7.64
Diluted a-Si:H—our values	14.42	0.982	0.559	7.92
Undiluted a-Si:H—delft values	15.59	0.816	0.610	7.76

TABLE III. Performances obtained by approximating the three pairs of Gaussian distributions D^+, D^0, and D^- in the intrinsic layer by one pair of Gaussians D, for three different sets of parameters.

	J_{SC} (mA/cm^2)	V_{OC} (V)	FF	η (%)
Undiluted a-Si:H—Delft values	15.72	0.814	0.609	7.79
Diluted a-Si:H—Liang *et al.*	14.18	0.953	0.566	7.64
Diluted a-Si:H—our values	14.41	0.982	0.560	7.92

was assumed equal to 0.2 eV (Ref. 17) (see the first column of Table I). Liang *et al.* do not give details of the distribution of defects used in their simulations. AMPS-1D allows for a maximum of two pairs of Gaussian distribution of defect states: two with donor-like and two with acceptor-like states. The simplest representation, extensively used more than one decade ago, included one Gaussian distribution with donor-like and another with acceptor-like states that here will be recognized as G_D and G_A.[17] The light J-V curves obtained with D-AMPS with one pair of Gaussians are shown in Table III. The density of states inside each Gaussian distribution G_D and G_A was adopted equal to the sum of the densities of states enclosed by the three Gaussian distributions D^-, D^0, and D^+ (spaced 0.3 eV) and the correlation energy was increased from 0.2 to 0.4 eV. The standard deviations of G_D and G_A were assumed twice as big as the ones of D^-, D^0, and D^+, and capture cross sections were assumed identical. The first line of Table III should be compared with the last line of Table II, and the last two lines of Table III with the second and third lines of Table II. As can be seen, the predicted light J-V curves did not show much discrepancies when the density of defect states was modeled with either three pairs or with only one pair of Gaussian distributions. Deviations obtained in the simulated dark J-V curves were not significant either. Having shown this, for solar cells in the initial state, the more accepted formalism with three-Gausians D^-, D^0, and D^+ will be used in the rest of this work.

Figure 2 shows the solar cell performance as a function of the density of defects for the three sets of parameters listed in Table I. As can be seen, J_{SC}, V_{OC}, FF, and η decline more markedly with the defect density when the parameters of Liang *et al.* are used. Figure 2(d) shows that the efficiency can be assumed independent of the defect density when this parameter is approximately lower than 1–5 $\times$ 10^{14} cm^{-3} for

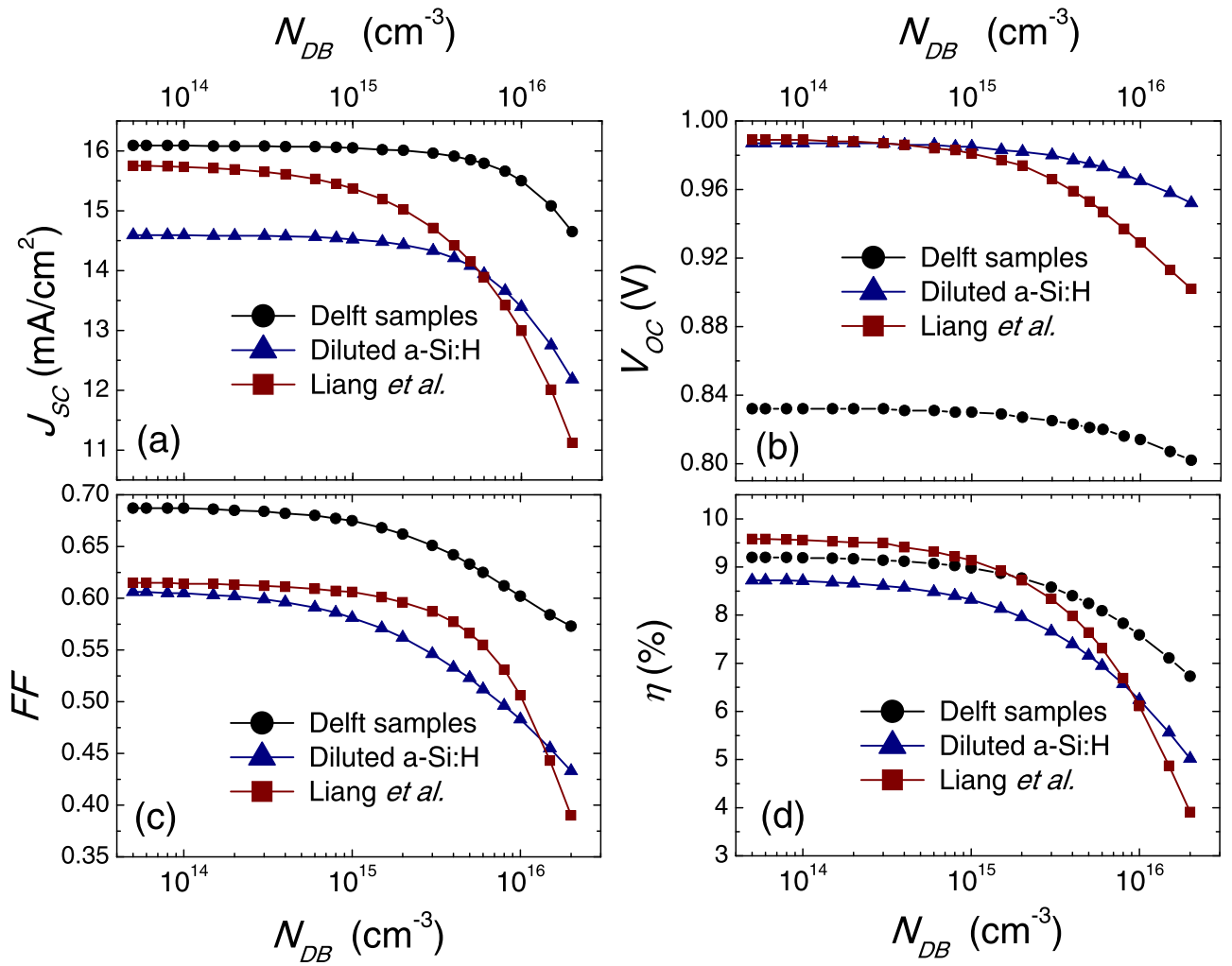

FIG. 2. Solar cell performance, characterized by (a) short circuit current density, J_{SC}, (b) open circuit voltage, V_{OC}, (c) fill factor, FF, and (d) efficiency, η, as a function of the density of defects in the intrinsic layer of an a-Si:H *p-i-n* solar cell obtained with: our parameters for undiluted (*i*)-a-Si:H (black circles, see the second column of Table I); Liang *et al.*'s parameters (red squares, see the third column of Table I); and our parameters for diluted (*i*)-a-Si:H (blue triangles, see the fourth column Table I). The intrinsic layer is 893 nm thick.

the three sets of parameters. The predicted dependences obtained with our parameters are similar for either undiluted or diluted a-Si:H samples. On the other hand, the decline of the solar cell efficiency with the defect density is more pronounced when Liang *et al.*'s parameters are used (Fig. 2(d)).

B. Impact of Liang *et al.* parameters on light *J-V* curves

Naturally, electrical parameters used by different groups working on a-Si:H solar cell modeling show some spread.[11–14,16–22] However, the electrical parameters of Liang and Schiff[4,15,23] have two unusual features: a considerably higher density of states at mobility edges ($G_{AO} = 1.6 \times 10^{22}\,cm^{-3}$ and $G_{DO} = 6 \times 10^{21}\,cm^{-3}$) with narrower tails ($E_A = 20$ meV and $E_D = 40$ meV) and poor free carrier mobilities ($\mu_N = 2\,cm^2\,V^{-1}\,s^{-1}$ and $\mu_P = 0.3\,cm^2\,V^{-1}\,s^{-1}$). These unusual parameters have a significant impact on the predicted *J-V* characteristics. The slope of the valence band tail E_D was assumed of only 40 meV by Liang and Schiff in some of their contributions,[4,5] but the value $E_D = 48$ meV was used in other papers.[23] The low slope of 40 meV was justified by limitations in the available version of AMPS-1D that allowed for changes of E_D in steps of 10 meV. The lowering of E_D from 48 meV to 40 meV significantly impacts the predicted solar cell performance, being E_D usually assumed between 44 and 50 meV in the literature.[13,14,18,19,23] Table IV shows the solar cell performances predicted with D-AMPS when our electrical parameters, obtained from fittings of *J-V* curves of a-Si:H *p-i-n* devices grown at Delft University, were replaced one at a time by the values proposed by Liang *et al.*[4] Although we performed simulations for solar cells with different thicknesses of the intrinsic layer, only results for the 893-nm-thick layer are presented in Table IV, as in Ref. 4.

TABLE IV. Changes obtained in the predicted solar cell performance of a-Si:H *p-i-n* solar cells with the 893-nm-thick intrinsic layer when our electrical parameters (second column of Table I) are replaced by the ones proposed by Liang *et al.*[4] One parameter is changed at a time. Cumulative effects are shown at the last line. Optical parameters were assumed identical in all cases.

Parameters	J_{SC} (mA/cm^2)	V_{OC} (V)	FF	η (%)
As in second column of Table I	15.59	0.8159	0.6102	7.762
$G_{AO} = 1.6 \times 10^{22}\,cm^{-3}$	15.62	0.8113	0.6072	7.694
$E_A = 20$ meV	15.59	0.8163	0.6107	7.770
$G_{DO} = 6 \times 10^{21}\,cm^{-3}$	14.53	0.7992	0.5608	6.511
$E_D = 40$ meV	15.73	0.8221	0.6348	8.207
$\sigma_{ND\text{-}T} = \sigma_{PA\text{-}T} = 10^{-16}\,cm^2$	15.46	0.8240	0.6112	7.787
$\sigma_{NA\text{-}T} = \sigma_{PD\text{-}T} = 1.3 \times 10^{-16}\,cm^2$	15.57	0.8152	0.6077	7.712
$\sigma_{ND\text{-}G} = \sigma_{PA\text{-}G} = 4 \times 10^{-15}\,cm^2$	15.71	0.8168	0.6193	7.948
$\sigma_{NA\text{-}G} = \sigma_{PD\text{-}G} = 7.5 \times 10^{-16}\,cm^2$	15.29	0.8064	0.5833	7.194
$DB = 5 \times 10^{15}\,cm^{-3}$	15.85	0.8213	0.6330	8.240
$DB = 10^{15}\,cm^{-3}$	16.05	0.8298	0.6745	8.984
$DB = 5 \times 10^{14}\,cm^{-3}$	16.07	0.8312	0.6811	9.097
$DB = 10^{14}\,cm^{-3}$	16.09	0.8323	0.6865	9.192
$DB = 5 \times 10^{13}\,cm^{-3}$	16.09	0.8325	0.6872	9.204
$N_C = N_V = 4 \times 10^{20}\,cm^{-3}$	15.61	0.8091	0.6085	7.684
$E_G = 1.74$ eV	15.63	0.8252	0.6171	7.959
$\mu_N = 2\,cm^2\,V^{-1}\,s^{-1}$	14.31	0.8115	0.5005	5.811
$\mu_P = 0.3\,cm^2\,V^{-1}\,s^{-1}$	12.91	0.8211	0.5671	6.013
$\mu_P = 0.2\,cm^2\,V^{-1}\,s^{-1}$	12.48	0.8211	0.5605	5.743
All changes together	11.92	0.8270	0.4796	4.728

The list of Liang *et al.*[4] was completed by assuming capture cross sections at tail and defect states similar to their counterparts because some values were missing. Table IV indicates that for the solar cells deposited at Delft University the most dramatic departure from our fittings is taking place when the low free carrier mobilities proposed by Liang *et al.* are assumed. The predicted *FF* becomes very poor, especially when the free electron and hole mobility are simultaneously lowered to $2\,cm^2\,V^{-1}\,s^{-1}$ and $0.3\,cm^2\,V^{-1}\,s^{-1}$, respectively. It is interesting to see that when the density of states at band edges is increased, only the valence band edge state density has a significant impact on the solar cell performance. Schiff[23] has even proposed higher values for the density of states at the valence band edge, of 10^{22} and $2 \times 10^{22}\,cm^{-3}\,eV^{-1}$, that would lead to an unacceptable very low *FF*, especially when the density of defects is evaluated with the Defect Pool model.[17] On the other hand, the conduction band edge state density can be increased one order of magnitude without significantly changing the predicted device characteristics. Changes in the light *J-V* due to modifications in the effective density of states and mobility gap are minor. Lower tail slopes and capture cross sections are bringing the expected improvement in the predicted solar cell performance. Table IV also includes the obtained solar cell performances when the density of defects is lowered in successive steps. Table IV shows that adopting the 1% criteria of tolerating a maximum of 1% in the deterioration of the solar cell efficiency with the increase of the density of defect states, the DB density should not be higher than $\sim 1 \times 10^{14}\,cm^{-3}$ in order to have solar cell performances controlled by tail states. Figure 2 also indicates that the solar cell efficiency approximately saturates at a density of defects of $\sim 10^{14}\,cm^{-3}$.

Next, the impact on the predicted *J-V* characteristics when our electrical parameters are replaced by those proposed by Liang *et al.*[4] is discussed in detail. In Fig. 3, we present calculations performed with D-AMPS for a *p-i-n* solar cell with the 893-nm-thick intrinsic layer for the maximum power point condition. Figure 3(a) shows the band diagram, Fig. 3(b) the positive and negative trapped charge, Fig. 3(c) the electric field distribution, and Fig. 3(d) the recombination rate. In all cases, solid lines present the situation when our parameters (second column of Table I) are used. The total density of acceptor- and donor-like tail states is given by the product $G_{A0}E_A$ and $G_{D0}E_D$, respectively. However, higher DOSs at the mobility edge combined with lower band tail slopes do not lead to equivalent results. Effective recombination centers are located between the demarcation energies defined by Rose[24] (located close to the quasi-Fermi levels, see Fig. 3(a)). The most significant contributions to recombination losses at the intrinsic layer, that determine to a great extend V_{OC}, take place at donor-like tail and defect states.[13] The contribution of acceptor-like tail states is not significant due to the steeper conduction tail slope.[13] Using the 1% criterion for the solar cell efficiency and assuming $E_A = 30$ meV (second column of Table I),

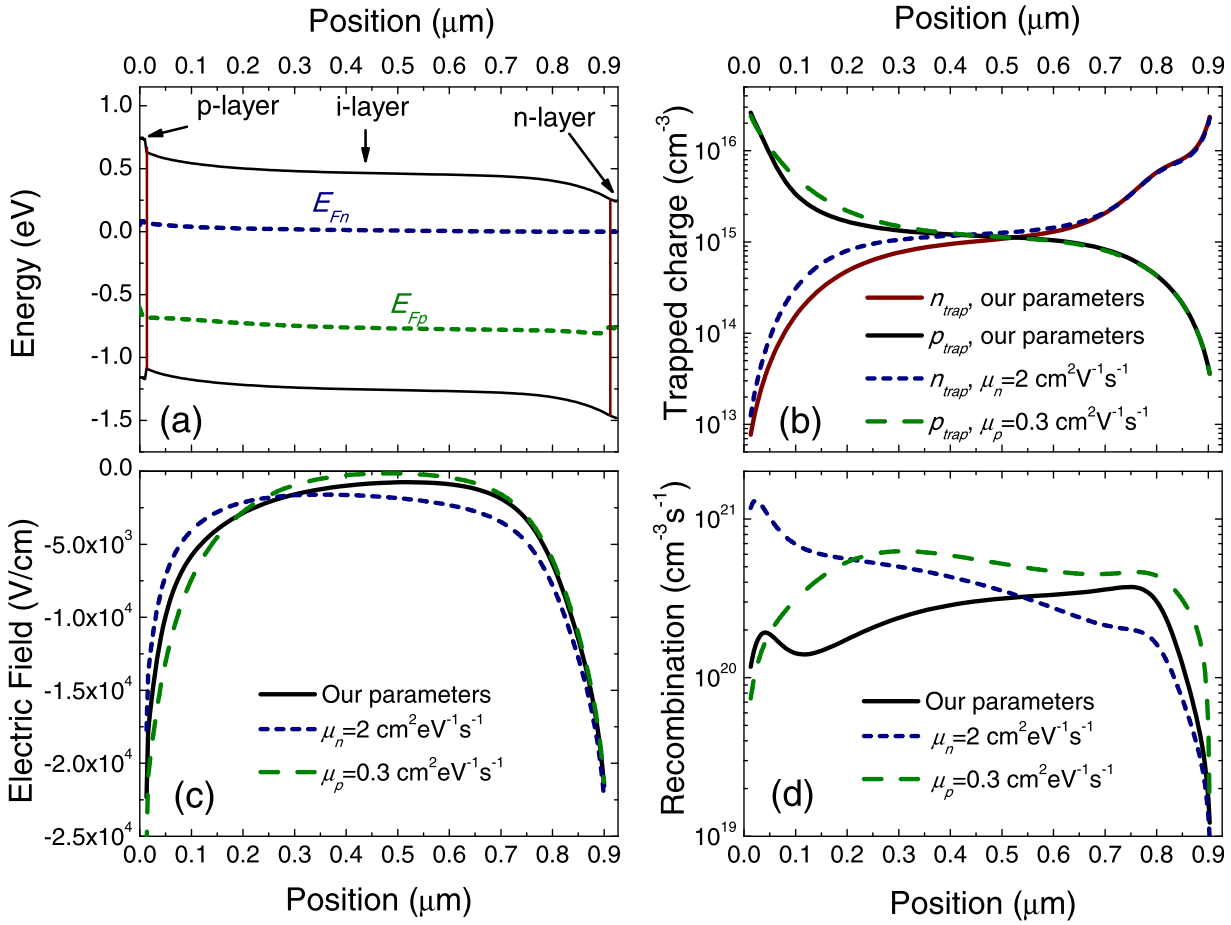

FIG. 3. Position dependence of (a) band edges and quasi-Fermi levels, (b) trapped positive (p_{trap}) and negative (n_{trap}) charge, (c) electric field, and (d) recombination rate; calculated with D-AMPS for a *p-i-n* solar cell under AM1.5 illumination and maximum power point condition. In (b)–(d), solid lines correspond to the situation when our parameters (second column of Table I) are used, dotted lines when μ_N is lowered to 2 cm^{2}V^{-1}s^{-1}, and dashed lines when μ_P is lowered to 0.3 cm^2 V^{-1} s^{-1}, as suggested by Liang *et al.*[4] One parameter is changed at a time.

the solar cell performance becomes sensitive to acceptor tail-states when the DOS at the conduction band edge is 2×10^{22} cm^{-3} eV^{-1} or higher. Hence, this particular choice of Liang *et al.*[4] does not have a significant impact in our simulations. Something similar can be said about lowering the conduction band tail slope to $E_A = 20$ meV. On the other hand, the increase of G_{D0} to 6×10^{21} cm^{-3} eV^{-1} gives rise to a significant enhancement of the recombination rate and trapped hole concentration, especially under AM1.5 illumination, due to the wider slope of the valence band tail and the lower mobility of holes. Recombination through donor-like tail states dominates the total recombination rate, but the contribution of defect states remains non negligible even for $G_{D0} = 6 \times 10^{21}$ cm^{-3} eV^{-1}. The additional positive charge hosted at a higher number of donor-like tail states is more significant in the front region of the intrinsic layer and gives rise to a redistribution of the electric field that becomes stronger near the *p*/*i* interface and weaker at the bulk intrinsic layer due to partial electrical shielding. The higher recombination rate, combined with a weaker electric field, gives rise to *p-i-n* a-Si:H solar cells with lower *FF* and J_{SC}, and to a lesser extent to lower V_{OC}, and poorer conversion efficiencies (see Table IV). The opposite trend is obtained when the slope of the valence band tail is reduced to $E_D = 40$ meV. In this case, the recombination in the intrinsic layer becomes controlled by defect states for $G_{D0} = 10^{21}$ cm^{-3} (see Table IV).

The low free carrier mobilities assumed by Liang *et al.*[4] also have important consequences on the predicted solar cell performances. When the electron mobility is lowered, the concentration of free electrons increases, favoring electron trapping and recombination. The concentration of trapped negative charge is significantly increased in the front region of the device (Fig. 3(b), dotted line), causing an important redistribution of the electric field that becomes weaker (stronger) in the front (back) region of the intrinsic layer (Fig. 3(c), dotted line). The higher concentration of free electrons and the electric field redistribution considerably enhance the recombination rate in the front region of the intrinsic layer, where electrons are minority carriers (Fig. 3(d), dotted line). The final result is a considerable deterioration of J_{SC}, *FF*, and η, while V_{OC} remains comparable (see Table IV). When the hole mobility is lowered, the concentration of free holes is increased, favoring hole trapping and recombination. The concentration of trapped positive charge is significantly increased in the front region of the device (Fig. 3(b), dashed line), and the opposite redistribution of the electric field takes place, becoming weaker (stronger) in the bulk (front) region of the intrinsic layer (Fig. 3(c), dashed line). The higher concentration of free

holes and the electric field redistribution considerably magnify the recombination rate in the bulk of the intrinsic layer, where holes are minority carriers (Fig. 3(d), dashed line). The final result is also an important deterioration of J_{SC}, FF, and η, while V_{OC} is only slightly modified (see Table IV).

Changes in the predicted performances are obtained when capture cross sections at donor tail-states are modified. The contribution of acceptor tail-states is quite minor. The reduction of $\sigma_{ND\text{-}T}$ allows for more positive charge trapped at donor-like tail states, giving rise also to a redistribution of the electric filed that becomes stronger near the p/i interface. The reduction of $\sigma_{ND\text{-}T}$ makes the total recombination rate in the intrinsic layer to become controlled by defect states, and dominated by donor (acceptor) defect states in the front (back) region of the intrinsic layer.[13] The magnification (deterioration) of the electric field in the front (back) region of the intrinsic layer decreases (increases) the recombination through donor (acceptor) defect states. The final results are slight changes in V_{OC}, FF, and J_{SC}. The increase of $\sigma_{PD\text{-}T}$ proposed by Liang *et al.*[4] is minor and no discussion is needed. When capture cross sections at either charged donor or acceptor defect sates are decreased (see Table IV), the predicted solar cell performance is affected. The reduction of $\sigma_{ND\text{-}G}$ and $\sigma_{PA\text{-}G}$ diminishes the recombination losses at defect states and gives rise to a minor redistribution of the electric field. The final result is a minor improvement of J_{SC}, V_{OC} and FF. On the other hand, when capture cross sections at neutral defect sates are increased both the recombination rate and charge trapping are favored. Lower J_{SC}, V_{OC}, and FF are obtained and changes are a bit more significant.

When the effective density of states N_C and N_V is increased, more extended states are available to host the free carriers, favoring higher concentrations of free holes and electrons, especially near the exit contacts. In the bulk, quasi-Fermi levels are further apart from band edges, giving rise to lower concentrations of trapped carriers at band tails and higher concentrations at defect states. This charge redistribution gives rise to higher electric fields near the interfaces and lower electric fields in the bulk. Interestingly, the recombination rate increases near the interfaces and decreases in the bulk. When the mobility gap is increased, the effect is practically the opposite, because the free carrier concentrations become lower. Emission coefficients are reduced by the wider energy separation between defect states and band edges. Trapped carrier concentrations at defect states are also lowered because quasi-Fermi levels depart more from the mid-gap. Hence, the electric field is weakened (strengthened) in the front (back) region of the intrinsic layer. The overall recombination is lowered, and higher V_{OC} is obtained because a higher injection of free carriers will be needed to counteract the optical generation rate. In any case, for these parameters the differences between ours and Liang *et al.*[4] values are quite low.

When our parameters are replaced by the ones of Liang *et al.*,[4] similar trends are obtained in the performances of a-Si:H *p-i-n* devices with different thicknesses of the intrinsic layer, with few exceptions. Let's note for instance that, when the electron mobility is reduced, there is a more significant deterioration of the FF in the cell with the 893 nm thick intrinsic layer than in thinner cells. The performance of thicker solar cells is more sensitive to modifications in the electrical parameters.

C. Transport mechanism shaping the *J-V* curves

The dark current of a-Si:H based *p-i-n* devices at low-forward voltages is limited by recombination through defect states,[25] while at intermediate forward voltages (inside the exponential region of the *J-V* curve) is limited by a combination of recombination through defect and tail states and free carrier diffusion. At high forward voltages, over the knee of the exponential region of the *J-V* curve, the device enters into the Space Charge Limited Current (SCLC) regime where the virtual cathode limits the injection of electrons into the intrinsic layer.[26] The contribution of tail states to recombination and trapping becomes significant at forward voltages over 0.7–0.8 V, where quasi-Fermi levels are separated enough to enter into the tails. In the SCLC regime, both tail and defect states impact the final trapped carrier concentrations and the recombination rate.

Under illumination and below V_{OC}, the current is given by the difference between the photo-current and the recombination losses taking place in the intrinsic and doped layers. The electron back diffusion loss at the front contact is comparatively low due to the presence of the wide-gap *p*-layer. Hole back diffusion at the back contact is always negligible. Under illumination but above V_{OC}, the device also enters into the SCLC regime, but the virtual cathode and anode are now tailored not only by injected carriers through contacts but also by photo-generated carriers trapped along the whole device. Hence, trapping and recombination taking place at defect and tail states impact the final shape of light *J-V* characteristic curves.[26]

IV. RECOMBINATION LOSSES AT TAIL AND DEFECT STATES

Liang *et al.*[4] concluded that P_{MAX} and V_{OC} of their as-deposited cells were not influenced by the presence of defect states, because otherwise the obtained P_{MAX} and V_{OC} would be noticeably below their calculated values, and the calculated $P_{\mathrm{MAX}}/J_P(-2\,V)$ obtained with a density of states where only defect states are taken into account would decrease as the temperature increases, while the measured and the calculated $P_{\mathrm{MAX}}/J_P(-2\,V)$ increase with temperature. They adopted a very unusual distribution of defect states: a donor-type 0/+ deep level without specifying its energy. The presence of acceptor-like defect states was not acknowledged.[4] However, defects in a-Si:H show a continuous (not discrete) distribution of states inside the mobility gap.[17]

Using the continuity equation, the current density J can be expressed as[27]

$$J = J_{N0} + J_{PL} + q\int_0^L R(x)\,dx - q\int_0^L G(x)\,dx, \qquad (1)$$

where J_{N0} is the electron back diffusion current at the front contact ($x=0$), J_{PL} is the hole back diffusion current at the back contact ($x=L$), $R(x)$ and $G(x)$ are the recombination

TABLE V. Electron back diffusion at the front contact (J_{N0}), recombination losses in the *p*-layer (R_P), intrinsic layer (R_I), and *n*-layer (R_N), and hole back diffusion at the back contact (J_{PL}), at short circuit (J_{SC}), maximum power (*FF*), and open circuit voltage (V_{OC}) conditions. The photocurrents are also shown for each device layer: (G_P), (G_I), and (G_N). The column "All" is the sum of the recombination and back diffusion losses and J_{PH} is the total device photocurrent. The assumed electrical parameters were listed in the second column of Table I. The intrinsic layer is 893 nm thick. All values are expressed in mA/cm^2.

Condition	J_{N0}	R_P	R_I	R_N	J_{PL}	All
J_{SC}	0.278	0.028	0.705	0.170	0.009	1.190
FF	0.405	0.043	3.740	0.195	0.009	4.392
V_{OC}	3.860	0.361	12.32	0.225	0.009	16.78
		G_P	G_I	G_N		J_{PH}
G		0.774	15.82	0.184		16.78

and optical generation rates, respectively, at the position "*x*" integrated along the device thickness *L*, and *q* is the electron charge. The integrals can be expressed as sum of the contributions originated in each device layer (*p*-, *i*-, and *n*-). Table V shows the contact and recombination losses and the optical currents obtained at the three layers of the a-Si:H *p-i-n* solar cell with an 893 nm thick intrinsic layer using the parameters obtained from our fittings.[13] Inspection of Table V indicates that the recombination loss in the intrinsic layer (R_I) changes more rapidly with the applied forward voltage and is the most significant at maximum power and open voltage conditions.

Table VI shows how the recombination losses are distributed between tail and defect states in the 893 nm thick intrinsic layer of the a-Si:H *p-i-n* solar cell at short circuit, maximum power, and open circuit voltage conditions, with our and Liang *et al.*'s parameters, assuming a density of defects of $9 \times 10^{15}\,\mathrm{cm}^{-3}$. The last column of Table VI shows the ratio between the recombination losses taking place at defect and tail states, defined as $R_{DT} = R_{DEF}/R_{TAIL}$. Table VI indicates that the performance of a-Si:H solar cells in the initial state is indeed more affected by defect states than by tail states. Similar conclusions were obtained for the *p-i-n* samples grown at Delft University with intrinsic layer thicknesses of 200, 400, and 600 nm.[13] The solar cell performance could be considered entirely controlled by tail states when R_{DT} is 0.1 or lower. Table VI includes some results for lower defect densities. These calculations show again that defect densities not higher than $10^{14}\,\mathrm{cm}^{-3}$ are needed to have the certainty that the solar cell performance is controlled by tail states.

TABLE VI. The symbols J_{SC}, *FF*, and V_{OC} correspond to short circuit, maximum power, and open circuit voltage conditions, respectively, R_{TAIL} and R_{DEF} are the recombination losses, expressed in mA/cm^2, taking place at tail and defect states of the *p-i-n* (*n-i-p*) device with an 893-nm-thick intrinsic layer. The right column shows the ratio $R_{DT} = R_{DEF}/R_{TAIL}$ between the recombination losses at defect and tail states. When not mentioned, the density of DBs was assumed to be $9 \times 10^{15}\,\mathrm{cm}^{-3}$.

Parameters	Condition	R_{TAIL} (mA/cm^2)	R_{DEF} (mA/cm^2)	R_{DT}
Liang *et al.*	J_{SC}	0.442	3.074	6.955
Liang *et al.*	*FF*	1.069	6.218	5.817
Liang *et al.*	V_{OC}	4.051	13.42	3.313
Ours	J_{SC}	0.113	0.592	5.239
Ours	*FF*	0.909	2.831	3.114
Ours	V_{OC}	4.453	7.872	1.768
Ours(DB = 5×10^{14})	J_{SC}	0.115	0.049	0.426
Ours(DB = 5×10^{14})	*FF*	1.824	0.458	0.251
Ours(DB = 5×10^{14})	V_{OC}	8.883	1.529	0.172
Ours(DB = 10^{14})	J_{SC}	0.118	0.013	0.110
Ours(DB = 10^{14})	*FF*	2.042	0.107	0.052
Ours(DB = 10^{14})	V_{OC}	9.559	0.455	0.048

Table VII shows the densities of defects needed to obtain $R_{DT} = 0.1$ at short circuit, maximum power, and open circuit voltage conditions, with ours and Liang *et al.*'s parameters. Defect densities between $10^{14}\,\mathrm{cm}^{-4}$ and $5 \times 10^{14}\,\mathrm{cm}^{-3}$, well below the figures reported in the literature, were obtained. Table VII also shows that using Liang *et al.*[4] parameters, lower defect densities than the ones obtained with our parameters would be needed to make recombination losses (and therefore J_{SC}, *FF*, and V_{OC}) of a-Si:H based solar cells in the annealed state to be controlled by tail states. The obtained defect densities for $R_{DT} = 0.1$ are a bit higher in thinner intrinsic layers, due to the stronger electric field. Sub-gap absorption measured by Constant Photocurrent Method (CPM) showed little effect on the defect density of a-Si:H films grown with or without hydrogen dilution,[28] while similar experiments performed with Dual Beam Photoconductivity (DBP)[29] indicate that, although the neutral density of defects remains unaltered, the density of charged defects in hydrogen diluted samples decreased by a factor of ~3 to 4.

Table VIII shows the recombination losses obtained at tail and defect states in the 893-nm-thick intrinsic layer when our electrical parameters are replaced one at a time by the ones proposed by Liang *et al.*[4] The ratio R_{DT} remains always larger than one except when the density of states at the valence band G_{D0} is increased from $10^{21}\,\mathrm{cm}^{-3}\,\mathrm{eV}^{-1}$ to $6 \times 10^{22}\,\mathrm{cm}^{-3}\,\mathrm{eV}^{-1}$. When our electrical parameters are all simultaneously replaced by their counterparts of Liang *et al.*,[4] the recombination losses in the intrinsic layer become more controlled by defect states due to their choices for tail states capture cross sections and slopes. In Table VIII, identical doped layers as the ones used to match the *J-V* curves of samples deposited at Delft University were

TABLE VII. The symbols J_{SC}, *FF*, and V_{OC} correspond to short circuit, maximum power, and open circuit voltage conditions, respectively, *W*(i) is the intrinsic layer thickness. The right column shows the density of defects that gives $R_{DT} = 0.1$.

Parameters	*W*(i) (nm)	Condition	$DB_{density}$ (cm^{-3})
Liang *et al.*	893	J_{SC}	1.07×10^{14}
Liang *et al.*	893	*FF*	1.46×10^{14}
Liang *et al.*	893	V_{OC}	1.14×10^{14}
Ours	893	J_{SC}	1.42×10^{14}
Ours	893	*FF*	2.94×10^{14}
Ours	893	V_{OC}	4.25×10^{14}
Ours	600	J_{SC}	1.56×10^{14}
Ours	600	*FF*	3.10×10^{14}
Ours	600	V_{OC}	4.88×10^{14}

TABLE VIII. Impact on the recombination losses at tail and defect states taking place in the 893 nm thick intrinsic layer of a *p-i-n* cell when our electrical parameters (second column of Table I) are replaced by the ones of Liang *et al.* (third column of Table I). The symbols J_{SC}, FF, and V_{OC} correspond to short circuit, maximum power, and open circuit voltage conditions, respectively, R_{TAIL} and R_{DEF} are the recombination losses at tail and defect states expressed in mA/cm^2. The right column shows the ratio $R_{DT}=R_{DEF}/R_{TAIL}$. The lines with the words "all" show the effect of simultaneously using all the parameters of Liang *et al*. The lines (Ours-DPM) show the results when the density of defects is modeled with the Defect Pool Model.

Parameters	Condition	R_{TAIL} (mA/cm^2)	R_{DEF} (mA/cm^2)	R_{DEF}/R_{TAIL}
Ours	J_{SC}	0.113	0.592	5.24
Ours	FF	0.909	2.831	3.11
Ours	V_{OC}	4.453	7.872	1.77
$\mu_N=2\,cm^2V^{-1}\,s^{-1}$	J_{SC}	0.334	1.222	3.66
$\mu_N=2\,cm^2V^{-1}\,s^{-1}$	FF	1.411	3.379	2.39
$\mu_N=2\,cm^2V^{-1}\,s^{-1}$	V_{OC}	4.562	7.894	1.73
$\mu_P=0.3\,cm^2V^{-1}\,s^{-1}$	J_{SC}	0.889	2.538	2.85
$\mu_P=0.3\,cm^2V^{-1}\,s^{-1}$	FF	2.041	4.695	2.30
$\mu_P=0.3\,cm^2V^{-1}s^{-1}$	V_{OC}	4.450	7.399	1.66
$G_{A0}=1.6\times10^{22}\,cm^{-3}\,eV^{-1}$	J_{SC}	0.130	0.559	4.30
$G_{A0}=1.6\times10^{22}\,cm^{-3}\,eV^{-1}$	FF	1.140	2.536	2.22
$G_{A0}=1.6\times10^{22}\,cm^{-3}\,eV^{-1}$	V_{OC}	5.786	6.892	1.19
$G_{D0}=6\times10^{22}\,cm^{-3}\,eV^{-1}$	J_{SC}	0.963	0.873	0.91
$G_{D0}=6\times10^{22}\,cm^{-3}\,eV^{-1}$	FF	3.105	2.268	0.73
$G_{D0}=6\times10^{22}\,cm^{-3}\,eV^{-1}$	V_{OC}	9.147	4.502	0.49
$E_A=20\,meV$, $E_D=40\,meV$	J_{SC}	0.023	0.525	22.83
$E_A=20\,meV$, $E_D=40\,meV$	FF	0.244	2.967	12.16
$E_A=20\,meV$,$E_D=40\,meV$	V_{OC}	1.730	9.916	5.73
$E_G=1.74$ eV	J_{SC}	0.102	0.566	5.55
$E_G=1.74$ eV	FF	0.860	2.761	3.21
$E_G=1.74\,eV$	V_{OC}	3.897	7.326	1.88
$\sigma_T=1$–$1.6\times10^{-16}\,cm^2$	J_{SC}	0.032	0.829	25.90
$\sigma_T=1$–$1.6\times10^{-16}\,cm^2$	FF	0.231	3.834	16.60
$\sigma_T=1$–$1.6\times10^{-16}\,cm^2$	V_{OC}	0.962	10.23	10.63
$\sigma_G=5$–$7.5\times10^{-15\text{–}16}cm^2$	J_{SC}	0.115	0.774	6.73
$\sigma_G=5$–$7.5\times10^{-15\text{–}16}cm^2$	FF	0.754	3.236	4.29
$\sigma_G=5$–$7.5\times10^{-15\text{–}16}cm^2$	V_{OC}	3.590	9.389	2.62
$N_{C\text{-}V}=4\times10^{20}\,cm^{-3}$	J_{SC}	0.102	0.601	5.89
$N_{C\text{-}V}=4\times10^{20}\,cm^{-3}$	FF	0.830	2.913	3.51
$N_{C\text{-}V}=4\times10^{20}\,cm^{-3}$	V_{OC}	4.452	8.550	1.92
All	J_{SC}	0.175	4.910	28.06
All	FF	0.374	6.999	18.71
All	V_{OC}	0.753	10.73	14.25
Ours-DPM	J_{SC}	0.014	0.553	39.5
Ours-DPM	FF	0.248	3.420	13.79
Ours-DPM	V_{OC}	1.095	9.774	8.93

assumed. Table VIII also reveals that when free carrier mobilities are lowered, recombination losses at tails states tend to increase more rapidly than at defect states, but the contribution coming from defect states remains significant. Although the density of tail states proposed by Liang *et al*. is considerably higher at mobility edges, the tail slopes were reduced from 48 meV and 30 meV to 40 meV and 20 meV at the valence and conduction band tail, respectively. Using our parameters, only around $6.4\times10^{10}\,cm^{-3}$ acceptor-like tail states and $5\times10^{15}\,cm^{-3}$ donor-like tail states are located between the demarcation energies defined by Rose,[24] and therefore acting as effective recombination centers under short circuit conditions at the middle of the intrinsic layer. Using the parameters of Liang *et al*.[4] these numbers are around 8.1×10^{9} and $6.6\times10^{15}\,cm^{-3}$, respectively.

In this paragraph, using the information available in the literature and the electrical parameters of the doped layers of samples of Delft University (no information of the doped layers was available in the contribution of Liang *et al*.[4]), an attempt to match the light *J-V* curve of Liang *et al*.'s diluted a-Si:H solar cell with an 893 nm thick intrinsic layer was undertaken. Quoting the authors, the hydrogen dilution was carefully selected to maintain a good material quality throughout the entire intrinsic layer and avoid nano-crystallite inclusion.[4] It is widely accepted that hydrogen dilution widens the mobility gap of a-Si:H.[28–32] Some reports indicate little or no decrease in the density of defects,[28,33] while others indicate the contrary.[29–32] In the second case, evidence of lower defect densities was reflected in higher solar cell FF and V_{OC}.[30,31] In particular, in the paper of Yan *et al*.,[30] where the same collaborators of Liang were co-authors, the effect of hydrogen dilution in FF and V_{OC} was illustrated in their Table I. They showed characteristic parameters of light *J-V* curves measured under AM1.5 illumination at 25 °C on solar cells in the initial

state with a 200 nm thick intrinsic layer grown without, medium and high hydrogen dilutions. Their Table I (Ref. 30) shows V_{OC} of 0.956, 0.985, and 1.010 V, and FF of 0.675, 0.726, and 0.732 for cells deposited with three hydrogen dilution ratios; being the reported mobility gaps E_G 1.78, 1.80, and 1.84 eV, respectively,[30] all higher than 1.74 eV.[4] Interestingly, in the simulations of Yan *et al.*[30] performed also with D-AMPS-1D, the presence of a defect density of $10^{15}\,cm^{-3}$ was acknowledged. Higher capture cross sections at defect states and wider tail slopes were also adopted. Capture cross sections similar to our values of $10^{-14}\,cm^2$ and $10^{-15}\,cm^2$ at charged and neutral defect states, respectively, were also assumed. By adopting in our simulations a mobility gap E_G of 1.84 eV, the highest value mentioned by Yan *et al.*,[30] V_{OC} increased to 0.94 V. In order to enhance V_{OC} further, the following parameters were lowered: the effective density of states N_C and N_V to $4\times10^{19}\,cm^{-3}$, the density of defect states to $10^{15}\,cm^{-3}$,[26] the valence band tail slope and the density of defects at band edges to 45 meV and $7\times10^{20}\,cm^{-3}\,eV^{-1}$, respectively, as suggested by some measurements of the sub-gap absorption coefficient performed with the DBP technique.[29] The free electron and hole mobilities were assumed to be $10\,cm^2\,V^{-1}\,s^{-1}$ and $1\,cm^2\,V^{-1}\,s^{-1}$, respectively. In order to replicate the experimental results, the mobility gap had to be increased further to 1.88 eV and capture cross sections were slightly changed to $9\times10^{-15}\,cm^2$ and $9\times10^{-16}\,cm^2$ at defect states[28] and to $2\times10^{-15}\,cm^2$ and $2\times10^{-17}\,cm^2$ at tail states. Our results can be found in the last line of Table II, and the list of parameters in the last column of Table I. Assuming doped layers with higher conductivities would require lower mobility gaps in the intrinsic layer. The lower values of N_C, G_{AO}, N_V, and G_{DO} can be justified by the transition from a-Si:H to μc-Si:H when the hydrogen dilution rate is increased. In μc-Si:H, typical effective densities of states and density of states at band edges are around $3\times10^{19}\,cm^{-3}$ and $2\times10^{20}\,cm^{-3}\,eV^{-1}$, respectively.[34]

Finally, the last lines of Table VIII show the recombination losses obtained with our parameters in the *p-i-n* device with an 893-nm-thick non-diluted intrinsic layer when the defect density is modeled with the DPM.[17] The density of defects is highly non-uniform near the *p*/*i* and *i*/*n* interfaces, and flat in the bulk. The list of our input parameters can be found elsewhere.[35] The loss distribution in layers and contacts is also shown in Table VIII. The relative contribution of defect states to the total recombination rate in the intrinsic layer becomes much more significant with the DPM due to the higher concentration of defects present near the interfaces.

V. COMPARISON OF THE DARK AND LIGHT *J-V* CHARACTERISTICS OBTAINED WITH THE TWO SETS OF ELECTRICAL PARAMETERS

Figure 4 shows the changes obtained in the *J-V* characteristics under dark and illuminated (AM1.5 illumination) conditions when our parameters are replaced by the ones of Liang *et al.*[4] Only the parameters of the third column of Table I giving rise to significant modifications are included in Figure 4. Our fittings, obtained for the solar cell deposited at Delft University with a 600 nm thick intrinsic layer,[13] are indicated with open square symbols as guide for the eyes (see the second column of Table I).

Figure 4(a) shows that, when free carrier mobilities are lowered to the extent suggested by Liang *et al.*,[4] the high forward dark *J-V* declines significantly, and when the presence of defects is neglected the low forward dark *J-V* drops dramatically. Fittings of dark *J-V* curves in our previous publication[13] were performed up to 1 V. However, in a previous contribution a-Si:H *p-i-n* based solar cells in the annealed state prepared in a different laboratory were matched up to a forward voltage of 2 V, assuming electron and hole mobilities of $10\,cm^2\,V^{-1}\,s^{-1}$ and $0.88-1\,cm^2\,V^{-1}\,s^{-1}$, respectively.[26] Within the UDM formalism, the highest mobilities used by us in the intrinsic region of a-Si:H solar cells were

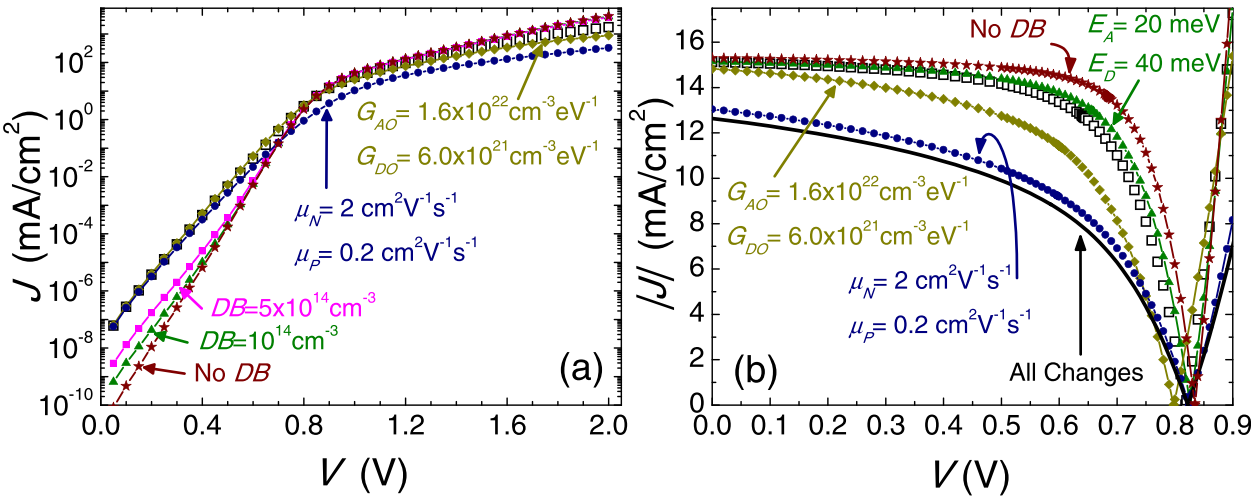

FIG. 4. Modifications obtained in (a) the dark and (b) the illuminated (AM1.5) *J-V* curves of the a-Si:H *p-i-n* solar cell with a 600 nm intrinsic layer, when our electrical parameters are replaced by the parameters suggested by Liang *et al.*[4] (see third column of Table I). The meaning of the symbols is as follows: (G_{A0},G_{D0}) density of states at the conduction and valence band edges; (μ_N,μ_P) electron and hole mobilities; (*DB*=) different concentrations of defects; (No *DB*) negligible density of defects in the intrinsic layer, (E_A,E_D) acceptor and donor band-tail slopes, (All changes) all the parameters of Liang *et al.* are adopted. Our fittings are indicated with open square symbols for comparison. In (b), the absolute value of the current density is plotted.

$\mu_n = 30\,cm^2\,V^{-1}\,s^{-1}$ and $\mu_p = 3\,cm^2\,V^{-1}\,s^{-1}$.[14] At high forward voltages, the current is limited by injection of electrons over the virtual-cathode barrier (SCLC regime). In *p-i-n* devices with good blocking contacts, the virtual cathode barrier is built up not only by electrons injected through the back contact but also by holes injected through the front contact.[26] When the electron and hole free carrier mobilities are lowered to $\mu_n = 2\,cm^2\,V^{-1}\,s^{-1}$ and $\mu_p = 0.3\,cm^2\,V^{-1}\,s^{-1}$, the low electron mobility favors trapping of electrons injected from the back contact at the virtual cathode, while the low hole mobility makes trapping of holes in the rear region of the device more difficult. The final result is a higher potential barrier at the virtual cathode that lowers the total current. At low forward voltages and under dark conditions, the quasi-Fermi levels cannot significantly enter into the tails, becoming recombination entirely controlled by defect states. Hence, the low forward dark *J-V* curve is very sensitive to the density and capture cross sections of defect states. On the other hand, the light *J-V* curve is more sensitive to the presence of tail states at any forward voltage, because electron-hole (*e-h*) pairs generated by the light source move the quasi-Fermi levels closer to the band edges even at low forward voltages. Recombination rates through tail and defect states become comparable. Our simulations indicate that the low forward dark *J-V* curve is insensitive to the presence of defects at densities of $\sim 10^{12}\,cm^{-3}$ or lower, while the light *J-V* curve is independent of the defect density for densities $\sim 1\text{–}5 \times 10^{14}\,cm^{-3}$ or lower. The dark current at low forward voltages becomes controlled by tail states for densities of defects below $10^{12}\,cm^{-3}$ because the density of states in the valence band tail near the mid-gap is $\sim 1.7 \times 10^{13}\,cm^{-3}$. Using Liang *et al.*[4] parameters, the equivalent density becomes $\sim 2.1 \times 10^{12}\,cm^{-3}$, indicating that a density of defects not higher than $2 \times 10^{11}\,cm^{-3}$ would be required to make the dark *J-V* curve insensitive to defect states. These very low densities of defects would give rise to saturation current densities below $10^{-9}\,mA/cm^2$ that were never reported. Although Liang *et al.*[4] only discussed the light *J-V*, it is interesting to stress that the dark *J-V* of a-Si:H *p-i-n* junctions is more sensitive to the presence of defect states than its counterpart, the light *J-V*.

Figure 4(b) shows that the deterioration of the solar cell performance when free carrier mobilities are lowered to the values suggested by Liang *et al.*[4] is quite considerable (blue circles). In addition, when the density of states is increased at the valence band edge as proposed by Liang *et al.* the solar cell efficiency also declines significantly (brown diamonds). The effect of using the whole set of parameters of Liang *et al.* is also shown (solid line). Figure 4(b) illustrates as well a slight improvement of the solar cell performance when the slopes of the band tails are reduced (green triangles), and a significant improvement when the density of defects is negligible (red stars). When the density of defects is lowered below $10^{14}\,cm^{-3}$ the recombination losses in the intrinsic layer become entirely controlled by tail states. Similar results were obtained for the predicted light and dark *J-V* characteristics of *p-i-n* solar cells in the annealed state when the intrinsic layer thickness is 893 nm.

VI. LIGHT *J-V* CHARACTERISTICS UNDER RED LASER ILLUMINATION

In this section, the light *J-V* curves are re-evaluated with D-AMPS with Liang *et al.*'s and with our parameters for a near-infrared (685 nm) laser light source of 30 mW (see Figure 5). A red or near IR laser light is more uniformly absorbed throughout the intrinsic layer than the AM1.5 source. However, the *e-h* pair generation profile is not entirely flat. In the solar cell with a 186 nm thick intrinsic layer, the generation rate at the *p/i* interface is only 1.014 higher than at the *i/n* interface, but in the solar cell with an 893-nm-thick intrinsic layer this factor is of 1.33. Our average generation rate *G* is a factor ~3.4 higher than $3.3 \times 10^{20}\,cm^{-3}$, the value used by Liang *et al.*[4] in their simulations, due to differences in the optical models and electrical parameters. The predicted light *J-V* curves for the four intrinsic layer thicknesses studied by Liang *et al.* indicate that, when the intrinsic layer density of defects is assumed to be $9 \times 10^{15}\,cm^{-3}$, the predicted *FFs* are quite poor. The saturation of the current, at least at room temperature and for the thickest solar cell, is not reached at $V = -2\,V$, contrary to the assumption of Liang *et al.*[4]

When the defect density is lowered to only $5 \times 10^{14}\,cm^{-3}$, the predicted *FF* obtained with Liang. *et al.*'s parameters is still poor for the solar cells with the thickest intrinsic layers. The predicted *FFs* were 0.726, 0.604, 0.479, and 0.447 for the 183, 377, 574, and 893 nm thick intrinsic layers, respectively, in comparison with 0.767, 0.736, 0.689, and 0.597 obtained with our parameters. For this low defect density, the current at reverse voltages approximately reaches saturation at $-2\,V$ even in the thickest solar cell. Hence, fittings of V_{OC} and the ratio between the maximum power density P_{MAX} and the current at a reverse voltage of $-2\,V$ can be preserved, but the matching of the full light *J-V* curves was not possible.

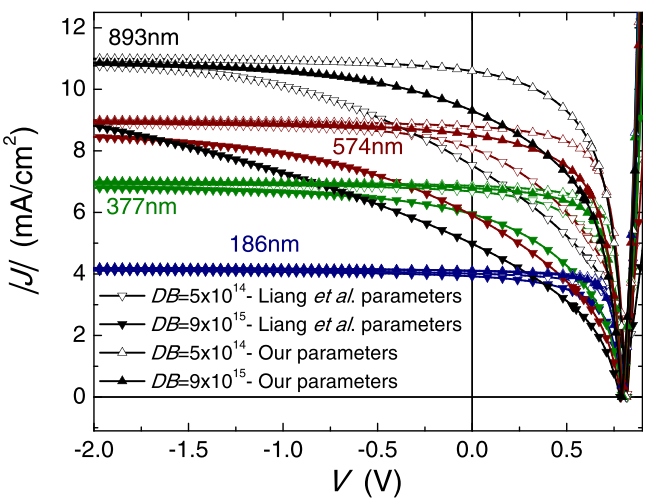

FIG. 5. Light *J-V* curves under red/near-IR laser illumination, obtained with D-AMPS for a-Si:H *p-i-n* solar cells with intrinsic layer thicknesses of 186 nm (blue symbols), 377 nm (green symbols), 574 nm (red symbols), and 893 nm (black symbols), when our parameters (second column of Table I, up triangle symbols) and Liang *et al.*'s[4] parameters (third column of Table I, down triangle symbols) are used. The global density of defects was assumed to be $5 \times 10^{14}\,cm^{-3}$ (open triangles) or $9 \times 10^{15}\,cm^{-3}$ (solid triangles). The current density is plotted in absolute value.

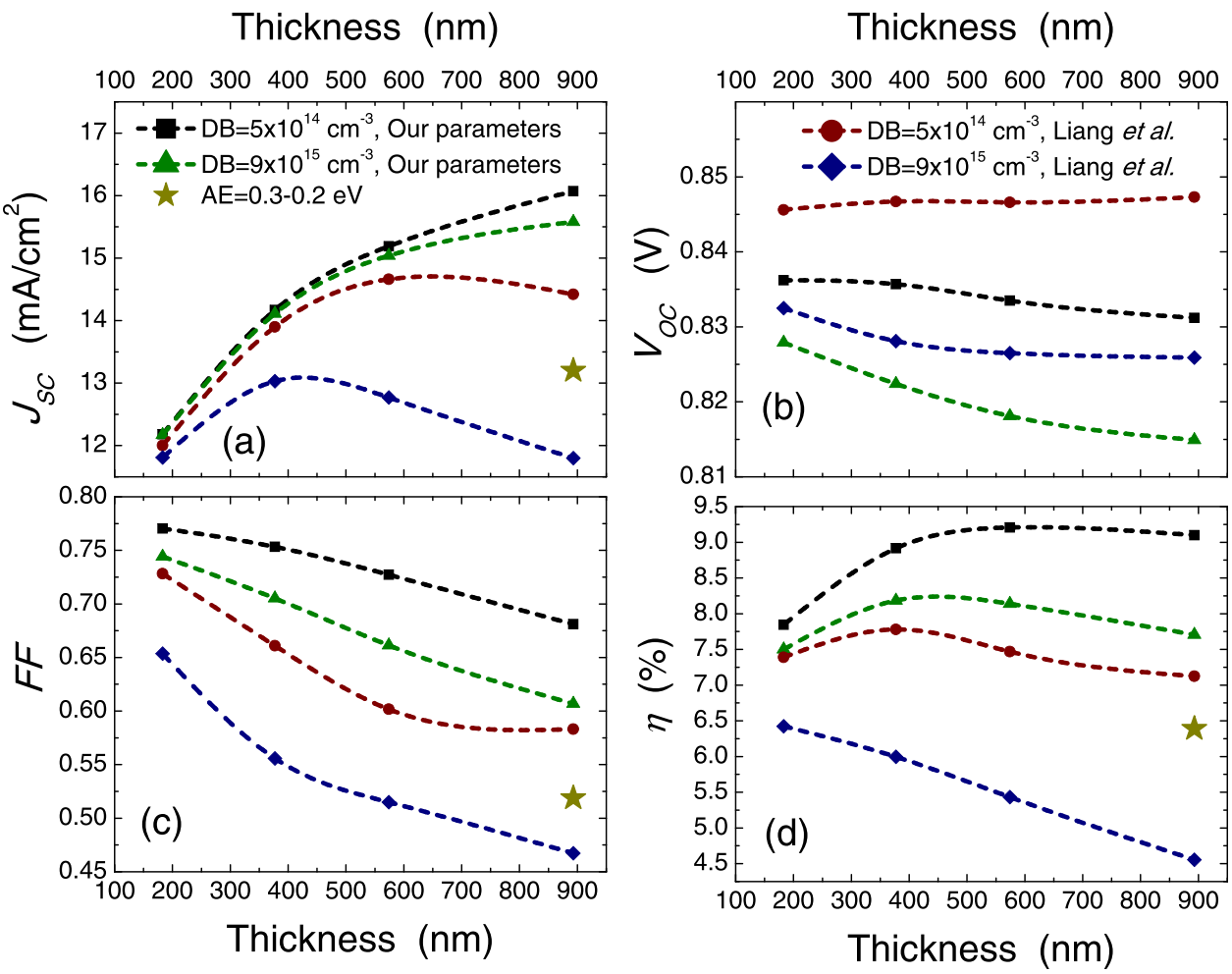

FIG. 6. Dependence of (a) short circuit current density, J_{SC}, (b) open circuit voltage, V_{OC}, (c) fill factor, FF, and (d) efficiency, η, as a function of the intrinsic layer thickness, calculated with D-AMPS for p-i-n solar cells under AM1.5 illumination, when our parameters (squares and triangles) or Liang *et al.*'s parameters (circles and diamonds) are used. Results are shown for two different densities of defects, $DB = 5 \times 10^{14}\,\mathrm{cm}^{-3}$ (squares and circles) and $DB = 9 \times 10^{15}\,\mathrm{cm}^{-3}$ (triangles and diamonds). The star symbol corresponds to a calculation made with Liang *et al.*'s parameters, a defect density of $9 \times 10^{15}\,\mathrm{cm}^{-3}$ and very optimistic activation energies of 0.3 and 0.2 eV at the p- and n-layer, respectively. V_{OC} results in this case 0.933 V, outside the range of (b). Lines are guide to the eye.

Identical conclusions were achieved by adjusting our generation rate G to $\sim 3.3 \times 10^{20}\,\mathrm{cm}^{-3}$ as in Ref. 4.

Figure 6 shows the performance of p-i-n solar cells under AM1.5 illumination calculated with D-AMPS for the four intrinsic layer thicknesses studied by Liang *et al.*[4] The short circuit current density (Fig. 6(a)) increases with thickness when our parameters are used (squares and triangles), but starts to decrease beyond a certain thickness when Liang *et al.* parameters are used (circles and diamonds). This point beyond which J_{SC} starts to decrease shifts to lower thicknesses as the defect density increases. The open circuit voltage (Fig. 6(b)) is not very sensitive to the intrinsic layer thickness, as expected. Figures 6(c) and 6(d) indicate that, with our parameters, the performance is similar to that experimentally observed in good-quality solar cells, while with Liang *et al.*'s parameters the cells exhibit poor FF and efficiencies, especially for intrinsic layers thicker than 400 nm, even for a density of defect states as low as $5 \times 10^{14}\,\mathrm{cm}^{-3}$ (circles). Assuming very optimistic activation energies of 0.3 and 0.2 eV in p- and n- layers, respectively, the solar cell performance could be significantly improved even for Liang *et al.* parameters and a defect density of $9 \times 10^{15}\,\mathrm{cm}^{-3}$ (see the point marked with a star in Fig. 6). For this particular case, the current density at $V = -2$ V is also near saturation. Hence, for a combination of good quality doped layers and lower defect densities in the intrinsic layer, the current density might reach saturation at $V = -2$ V.

VII. CONCLUSIONS

In as-deposited *a-Si:H* based solar cells grown without or with hydrogen dilution, our simulations indicate that V_{OC} and FF are controlled by recombination losses taking place through both tail and defect states located in the intrinsic layer. Our results also indicate that recombination losses at defect states are higher than at tail states, in contradiction with the results of Liang *et al.*[4]

The combination of low free carrier mobilities ($\mu_n = 2\,\mathrm{cm}^2\,\mathrm{V}^{-1}\,\mathrm{s}^{-1}$ and $\mu_p = 0.3\,\mathrm{cm}^2\,\mathrm{V}^{-1}\,\mathrm{s}^{-1}$) and high density of states at the valence band edge ($G_{DO} = 6 \times 10^{21}\,\mathrm{cm}^{-3}\,\mathrm{eV}^{-1}$), as suggested by Liang *et al.*,[4] did not allow the reproduction of the experimental light J-V curves of a-Si:H solar cells in the

annealed state deposited without hydrogen dilution. In solar cells with hydrogen diluted intrinsic layers, the fitting can be achieved with these parameters by invoking doped layers with unrealistic low activation energies.

The contribution of Liang *et al.*[4] shows fittings of V_{OC} and the ratio between the maximum power density P_{MAX} and the current J_P at a reverse voltage of $-2\,\mathrm{V}$, at different temperatures, for solar cells with four intrinsic layer thicknesses. Their results should be interpreted as successful replications of these two quantities, V_{OC} and $P_{\mathrm{MAX}}/J_P(-2\,V)$, but not of the entire experimental light J-V curves of the as deposited a-Si:H solar cells.

The photocurrent at $-2\,\mathrm{V}$ is not a good approximation of the saturated reverse-bias photocurrent in a-Si:H p-i-n solar cells at room temperature when the electron and hole mobilities and the density of states at the valence band mobility edge are assumed to be $\mu_n = 2\,\mathrm{cm^2\,V^{-1}\,s^{-1}}$, $\mu_p = 0.3\,\mathrm{cm^2\,V^{-1}\,s^{-1}}$, and $G_{DO} = 6\times10^{21}\,\mathrm{cm^{-3}\,eV^{-1}}$, respectively. Our simulations indicate that, at room temperature, the photocurrent drops significantly between $-2\,\mathrm{V}$ and $0\,\mathrm{V}$ in devices with 400 nm or thicker intrinsic layers.

ACKNOWLEDGMENTS

We highly appreciate the financial support from Agencia Nacional de Promoción Científica y Tecnológica through the Grant No. PICT-2013 2098. We would also like to thank members of the department of Photovoltaic Materials and Devices of Delft University of Technology, the Netherlands, for providing the experimental information, and to Dr. Marcelo de Greef for his help in fitting experimental data and in making the figures.

[1]C. R. Wronski, S. Lee, M. Hicks, and S. Kumar, Phys. Rev. Lett. **63**, 1420 (1989).
[2]F. Rubinelli, J. Hou, S. J. Fonash, C. R. Wronski, M. Bennet, and S. Wiedeman, in *Proceedings of the 22nd IEEE Photovoltaic Specialist Conference, Las Vegas* (1991), p. 1405.
[3]R. Kind, R. A. C. M. M. van Swaaij, F. Rubinelli, S. Solntsev, and M. Zeman, J. Appl. Phys. **110**, 104512 (2011).
[4]J. Liang, E. A. Schiff, S. Guha, B. Yan, and J. Yang, Appl. Phys. Lett. **88**, 063512 (2006).
[5]E. A. Schiff, J. Non-Cryst. Solids **352**, 1087 (2006).
[6]H. Zhu, A. K. Kalkan, J. Hou, and S. J. Fonash, AIP Conf. Proc. **462**, 309 (1999).
[7]S. J. Fonash, J. Arch, J. Hou, W. Howland, P. McElheny, A. Moquin, M. Rogosky, F. A. Rubinelli, T. Tran, and H. Zhu, *A Manual for AMPS-1D, A One-Dimensional Device Simulation Program for the Analysis of Microelectronic and Photonic Structures* (The Center for Nanotechnology Education and Utilization, The Pennsylvania State University, 1997).
[8]E. Klimovsky, J. K. Rath, R. E. I. Schropp, and F. A. Rubinelli, Thin Solid Films **422**(1–2), 211 (2002).
[9]E. Klimovsky, J. K. Rath, R. E. I. Schropp, and F. A. Rubinelli, J. Non-Cryst. Solids **338–340**, 686 (2004).
[10]F. A. Rubinelli, J. K. Rath, and R. E. I. Schropp, J. Appl. Phys. **89**, 4010 (2001).
[11]F. A. Rubinelli, R. Jiménez, J. K. Rath, and R. E. I. Schropp, J. Appl. Phys. **91**, 2409 (2002).
[12]F. A. Rubinelli, L. F. Marsal, and J. Pallarès, J. Appl. Phys. **97**, 034904 (2005).
[13]F. Rubinelli and H. Ramirez, J. Appl. Phys. **117**, 104513 (2015).
[14]M. de Greef, F. Rubinelli, and R. A. C. M. M. van Swaaij, Thin Solid Films **540**, 227 (2013).
[15]J. Yang, A. Banerjee, and S. Guha, Appl. Phys. Lett. **70**, 2975 (1997).
[16]H. Zhu, J. Yang, W. Wang, E. A. Schiff, J. Liang, and S. Guha, in *Amorphous and Nanocrystalline Silicon-Based Films*, edited by J. R. Abelson, G. Ganguly, H. Matsumura, J. Robertson, and E. A. Schiff (Mat. Res. Soc. Symp. Proc., 2003), Vol. 762, p. 297.
[17]M. Powell and S. Deane, Phys. Rev. B **48**, 10815 (1993).
[18]A. M. K. Dagamseh, B. Vet, P. Sutta, and M. Zeman, Sol. Energy Mater. Sol. Cells **94**, 2119 (2010).
[19]R. A. C. M. M. van Swaaij, R. Kind, and M. Zeman, J. Non-Cryst. Solids **358**, 2190 (2012).
[20]U. Duttam and P. Chaterjee, J. Appl. Phys. **96**, 2261 (2004).
[21]S. R. Dhariwal and M. Smirty, Sol. Energy Mater. Sol. Cells **90**, 1254 (2006).
[22]A. Mittiga, P. Fiorini, M. Falconieri, and F. Evangelisti, J. Appl. Phys. **66**, 2667 (1989).
[23]E. A. Schiff, Sol. Energy Mater. Sol. Cells **78**, 567 (2003).
[24]A. Rose, *Concepts in Photoconductivity and Allied Problems* (RCA Laboratories/Robert E. Krieger Publishing Co., Princeton, New Jersey/Huntington, NY, 1978).
[25]F. Rubinelli, J. Arch, and S. Fonash, J. Appl. Phys. **72**, 1621 (1992).
[26]F. A. Rubinelli, H. Liu, and C. R. Wronski, Philos. Mag. B **74**, 407 (1996).
[27]S. J. Fonash, *Solar Cell Device Physics*, 2nd ed. (Academic Press, Burlington, MA, USA, 2010).
[28]X. Xu, J. Yang, and S. Guha, J. Non-Cryst. Solids **198–200**, 60 (1996).
[29]Y. Lee, L. Hao, J. Koh, H. Fujiwara, Z. Lu, R. W. Collins, and C. R. Wronski, in *Amorphous and Microcrystalline Silicon Technology*, edited by M. Hack, E. A. Schiff, R. Schropp, I. Shimizu, and S. Wagner (Mat. Res. Soc. Symp. Proc., 1997), Vol. 467, p. 747.
[30]B. Yan, J. Yang, and S. Guha, Appl. Phys. Lett. **83**, 782 (2003).
[31]S. Guha, J. Yang, A. Banerjee, B. Yan, and K. Lord, Sol. Energy Mater. Sol. Cells **78**, 329 (2003).
[32]S. Guha, J. Yang, D. L. Williamson, Y. Lubianiker, J. D. Cohen, and A. H. Mahan, Appl. Phys. Lett. **74**, 1860 (1999).
[33]Q. Wang and R. Crandall, in *Amorphous and Microcrystalline Silicon Technology*, edited by M. Hack, E. A. Schiff, R. Schropp, I. Shimizu, and S. Wagner (Mat. Res. Soc. Symp. Proc., 1997), Vol. 467, p. 753.
[34]F. Rubinelli, Thin Solid Films **619**, 102 (2016).
[35]M. de Greef and F. Rubinelli, Phys. Status Solidi B **252**, 170 (2015).